JOURNAL OF GUIDANCE, CONTROL, AND DYNAMICS
Vol. 27, No. 6, November–December 2004

Test Results for Entry Guidance Methods for Space Vehicles

John M. Hanson*
NASA Marshall Space Flight Center, Huntsville, Alabama 35812
and
Robert E. Jones†
Sverdrup Technology, Inc., Huntsville, Alabama 35806

There are a number of approaches to advanced guidance and control that have the potential for achieving the goals of significantly increasing reusable launch vehicle (or any space vehicle that enters an atmosphere) safety and reliability and reducing the cost. This paper examines some approaches to entry guidance. An effort called Integration and Testing of Advanced Guidance and Control Technologies has recently completed a rigorous testing phase, where these algorithms faced high-fidelity vehicle models and were required to perform a variety of representative tests. The algorithm developers spent substantial effort improving the algorithm performance in the testing. This paper lists the test cases used to demonstrate that the desired results are achieved, shows an automated test scoring method that greatly reduces the evaluation effort required, and displays results of the tests. The primary contribution of the paper is to provide a quantitative comparison between the performance of five different entry guidance approaches. Results show a significant improvement over the current state of the art (shuttle-like guidance). The two best-scoring algorithm approaches show roughly equivalent results. Both can be expected to work well for future vehicle concepts.

Introduction

ADVANCED guidance and control has a significant potential to increase the safety of future reusable launch vehicles (RLV) and any space vehicles, as well as to reduce the cost of performing guidance and control analysis, both in the design and in the operational phases. This potential has been documented elsewhere.[1,2] It also has potential benefit for expendable vehicles. The benefit for expendables is less because modes of recovery that involve abort landings are not typically available. The improvement in safety results from the ability to adapt to unexpected significant off-nominal conditions and failure scenarios. The improvement in cost results from the ability to use the methods for varying vehicle models and mission scenarios without significant effort expended.

The Advanced Guidance and Control Project began in 1999 and had as its purpose to develop and test some of the potential methods. The concept was to consider as many openly available (not proprietary) entry guidance and ascent and entry control approaches as possible within the available resources. The algorithms had to be sufficiently advanced in development in order to support the test environment. The testing was performed in a high-fidelity simulation, against a number of stressing conditions, in order to discern the most flexible approaches. After 2001, the effort continued under the name Integration and Testing of Advanced Guidance and Control Technologies, with the goal to expand the effort to include all algorithm types within an advanced guidance and control architecture as well as all appropriate algorithm approaches.

The primary contribution of this paper is to provide results of quantitative testing of alternative entry guidance methods for purposes of comparison. This paper briefly describes the advanced approaches for entry guidance that are involved in the testing. We summarize an initial phase of testing performed to examine the various methods. Some lessons were learned from the initial phase of testing. Some of the algorithms performed well, but for the most part the methods were not ready to address all of the RLV needs. A second phase of testing was planned to more completely examine the performance of the algorithms vs the safety and cost requirements. This paper includes a description of the test cases for the second phase of testing. We also describe an automated method of scoring the algorithm performance that leads to a significant reduction of effort. Results are shown at the end of the paper. We also examine computational effort expended by the algorithms.

Although this paper is concerned with entry guidance testing, a complete architecture would include all phases of flight, with advanced guidance, control, and control allocation all included, as well as an automated mission manager to oversee the decision making for the guidance and control, and potentially a system identification module to identify how the behavior of the vehicle is different from the expected behavior. Integration into a complete architecture requires more than simply connecting the algorithms and making sure they work together. An example is a study[3] where an elevon failure during entry meant that the vehicle could not fly the nominal angle of attack profile because of insufficient control authority. The reaction control system (RCS) jets were not powerful enough to compensate for the failure, and the RCS fuel used would be excessive. However, by flying at a lower angle of attack, using RCS to help compensate for the loss of control, and redesigning the trajectory with the new angle of attack profile, it is possible to save the mission. Examples like this one show how these new methods can be used to advantage.

First Phase of Testing

An original goal in this effort was to include as many approaches as possible within the resources of the effort, with an eye toward not missing what might be the best approach. The methods had to be openly available and available with a relatively small budget. This led to an emphasis on university grants and in-house efforts.

A test series was conducted in September 2000. Four entry guidance methods were tested. The test environment was the X-33 Marshall Aerospace Vehicle Representation in C (MAVERIC) simulation.[4] MAVERIC was the only high-fidelity end-to-end simulation used for X-33 design. Its results impacted structural, thermal, and control system design. It was used to develop the ascent and entry guidance and control, as well as the flight mechanics portion of the mission manager. At the end of the X-33 Program, MAVERIC was matching the Integrated Test Facility simulation that

Presented as Paper 2004-0701 at the AIAA 42nd Aerospace Sciences Meeting, Reno, NV, 5–8 January 2004; received 14 May 2004; revision received 30 July 2004; accepted for publication 1 August 2004.

*Team Lead, Guidance, Navigation, and Control Group, TD54. Member AIAA.
†Senior Engineer, 6703 Odyssey Drive NW, Suite 303.

was to be used for verification of the flight software, in its all-digital mode.

The X-33 was planned to fly a number of suborbital test flights, so that these tests encompassed primarily ascent followed immediately by entry on suborbital trajectories. The suborbital flights can be viewed as representing different downrange aborts for a RLV. These tests are particularly stressing for entry guidance because the duration of the entry phase is short and because the entry guidance has to remove dispersions that result from the ascent phase. Additional tests were run for entry from various orbits, using the same simulation and vehicle models, with differing crossrange requirements and heat constraints.

Tests during phase 1 included different nominal missions, engine-out aborts, Monte Carlo dispersion runs for both nominal missions and aborts, and significant engine over and under performance. Failures and mismodeling not associated with the propulsion system were not explicitly considered for this phase 1 testing. Algorithm size, speed of execution, memory, complexity/effort required, and performance against a variety of criteria were all compared.

Of all of the methods tested in phase 1, the linear quadratic regulator (LQR)[5] entry guidance was the only one that performed quite well. In all cases (including LQR), it became clear that more work was necessary to develop the algorithms to their full potential, so that they would successfully fly the various test cases. This led to the definition of a second set of tests, as described below, and to more work on the algorithms, as described in the references. The manual examination of results performed during the phase 1 testing led to an automated test procedure for phase 2, as described later in this paper.

Methods to Be Examined

The work in this paper continues from work first described in Refs. 4 and 6. The following describes the different methods involved in this integration and testing.

1) The first is the baseline guidance method.[7] This method is like the shuttle entry guidance in that it tracks a nominal drag vs energy profile for longitudinal guidance and uses a heading error corridor to trigger periodic bank sign reversals for lateral guidance. It was the baseline entry guidance for X-33. The drag profile is stored as a piecewise linear function of energy. The nominal range-to-go calculation is a simple table lookup. Feedback linearization is used to define a tracking law for the drag profile. A damped harmonic oscillator model defines the desired time response, which is used to tune the guidance. Biasing of the terminal-area energy-management (TAEM) interface target and adjustment of the desired drag profile compensate for dispersions and cause the actual range to approximate the range that is obtained from flying the drag profile. TAEM is the flight phase that occurs after entry and is focused on setting up the landing phase. For this study, the TAEM interface is at about 762 m/s (2500 fps) relative speed, 55.56 km (30 nm) from the landing area, and at about 29 km (95,000 ft) altitude. Bank angle is the primary control, but modulation of angle of attack (within 5 deg of the nominal profile) is used, especially during bank reversals, to mitigate undesirable transient behavior. This guidance was used for a portion of the tests, for comparison purposes. It was not used for the complete set of tests because of the time it would have taken to set it up and tune it properly for all tests.

2) The linear quadratic regulator (LQR) method[5] has performed very well in test. The algorithm is of the reference-profile tracking type. The reference profile consists of reference states—range to go, altitude, and flight-path angle—and reference controls—bank angle and angle of attack vs energy. A linear control law using state feedback is used with energy-scheduled gains. The gains are obtained off-line using MATLAB's® steady-state LQR function. Lateral trajectory control is obtained through bank sign reversals chosen based on a heading error corridor. The algorithm is not quite as flexible as methods with onboard trajectory regeneration capability, but it is very robust with respect to varying initial conditions. The guidance gains are for the most part trajectory independent.

3) The numerical predictor-corrector method,[8] called Eguide by its developers, chooses parameters using a Newton procedure and numerical integration to obtain a desirable trajectory onboard for the actual flight conditions. Eguide follows a reference heat rate early in entry. A total of four parameters are chosen for entry: reference heat rate, initial bank angle, bank-angle rate, and the time to switch from heat rate tracking to targeting the TAEM interface. After the high heating region is passed, Eguide uses initial bank and bank rate to target the TAEM interface. Eguide contains a planning stage and also functions as guidance with a combination of a numerical predictor-corrector and a profile-follower using the LQR guidance just described. This method results in very smooth bank angle and angle-of-attack commands and a smooth altitude profile. A bank reversal is chosen to satisfy the lateral motion necessary to reach the TAEM interface.

4) The drag-energy three-dimensional method is an entry trajectory design and guidance procedure based on extension of the shuttle trajectory design methods to three dimensions.[9] We will refer to the method in this paper as drag-energy three dimensions. The method is called EAGLE by the authors, for evolved acceleration guidance logic for entry. The planning algorithm generates reference drag acceleration and lateral acceleration profiles, along with the reference state and bank-angle profiles. Drag-energy three dimensions chooses a drag profile using a three-segment linear spline fit for a profile that fits within the drag vs velocity constraints and gives the correct value for downrange distance. These constraints can include thermal, dynamic pressure, normal acceleration, and equilibrium glide constraints. The lateral motion is determined through a bank reversal chosen to minimize the final crossrange error. An iteration is used to improve the flight-path length and curvature estimates. A feedback linearization control tracks the reference drag and heading profiles.

5) The final method is a trajectory design method that uses quasi-equilibrium glide (shallow and nearly constant flight-path angle with varying bank angle), combined with a predictor-corrector method, to design a trajectory for entry.[10] We will refer to this method as quasi-equilibrium glide. The use of equilibrium glide during the high-heating portion of entry enables the inequality constraints to be observed. The entry trajectory design problem is decomposed into two sequential one-parameter search problems. The three-dimensional trajectory is derived (longitudinal and lateral motion) to ensure that the TAEM interface will be successfully reached. First, the motion for the initial entry into the atmosphere and the longitudinal profile for the pre-TAEM portion are found. Next, the method estimates the longitudinal profile for the high-heating quasi-equilibrium glide phase. Integrating the equations of motion enables the trajectory to converge and to follow the correct vehicle dynamics. The combined longitudinal motion satisfies the constraints and end conditions. A bank reversal is chosen to satisfy the lateral motion requirements. A profile-following guidance flies the trajectory, focusing on following all of the trajectory parameters.[11]

Test Cases and Test Criteria

For the second phase of tests, we included many of the first set of tests again because the methods (as they existed in the first phase of testing) did not in most cases perform satisfactorily. We also added tests for various failure and mismodeling cases that seemed appropriate. The test environment was a newer version of MAVERIC that models the X-33 vehicle in more detail and automates the required test processes. A list of the test cases follows in Table 1. Tests 22–25 are intended to approximate the effects of aerodynamic surface failures on the point mass [three degrees of freedom (DOF)] flight by restricting the maneuverability. That is, we assume the vehicle control is capable of still maintaining control, but the trajectory planning/guidance must accommodate a vehicle that is less maneuverable. To model these effects in detail, the resulting limited trim capability and the effects of modified trim lift and drag would be simulated accurately. To exercise the guidance, we approximate the reduction in maneuverability by restricting the angle of attack to a lower than planned value and by restricting maximum maneuvering rates to less than nominal. Table 2 shows the motivation for each set of tests.

Table 1 Entry guidance test series

Test number and description	DOF[a]	No. of runs
1) Mich10a1[b]	6	100 MCD[c]
2) Mich10a1, February environment, different random seed[d]	6	200 MCD
3) Mich10d1[b]	6	100 MCD
4) Mich10d1, August environment, different random seed	6	200 MCD
5) Mich10a1, PPO time 50 s (early abort to Michael)[e,f]	3	100 MCD
6) Mich10a1, PPO time 60 s	3	100 MCD
7) Mich10a1, PPO time 112 s	3	100 MCD
8) Mich10a1, PPO time 40 s (early abort to Ibex), different random seed[d,f]	3	200 MCD
9) Mich10d1, PPO time 38 s (early abort to Ibex), different random seed	3	200 MCD
10) Mich10a1, +4 sigma thrust dispersion from ascent	3	1
11) Mich10a1, +6 sigma thrust dispersion from ascent	3	1
12) Mich10a1, −12 sigma thrust dispersion from ascent	3	1
13) 51.6-deg ISS orbit entry, low crossrange, high peak heat rate limit, input profile to guidance is from this trajectory's design[g]	3	100 MCD
14) 51.6-deg ISS orbit entry, high right crossrange, high peak heat rate limit, input profile from 13	3	100 MCD
15) 51.6-deg ISS orbit entry, high left crossrange, high peak heat rate limit, input profile from 13	3	100 MCD
16) 51.6-deg ISS orbit entry, low crossrange, low peak heat rate limit, input profile from this trajectory's design	3	100 MCD
17) 51.6-deg ISS orbit entry, high right crossrange, low peak heat rate limit, input profile from 16	3	100 MCD
18) 51.6-deg ISS orbit entry, high left crossrange, low peak heat rate limit, input profile from 16	3	100 MCD
19) 28.5-deg LEO orbit entry, low crossrange, low peak heat rate limit, input profile from 16[h]	3	100 MCD
20) 28.5-deg LEO orbit entry, high right crossrange, low peak heat rate limit, input profile from 16	3	100 MCD
21) 28.5-deg LEO orbit entry, high left crossrange, low peak heat rate limit, input profile from 16	3	100 MCD
22) Mich10a1, aerosurface failure result: angle of attack limited to 5 deg less than nominal entry value	3	1
23) Mich10a1, aerosurface failure result: angle of attack and bank rates limited to 2 deg/s maximum	3	1
24) Mich10d1, aerosurface failure: angle of attack limited to 5 deg less than nominal entry value	3	1
25) Mich10d1, aerosurface failure: angle of attack limited to 5 deg less than nominal entry value, and angle of attack and bank rates limited to 2 deg/s maximum	3	1
26) Mich10a1, unknown to guidance, first flight aerodynamics mismodeling: aerodynamic lift coefficient 20% less than vehicle database model	3	1
27) Mich10a1, unknown to guidance, first flight aerodynamics mismodeling: aerodynamic drag coefficient 20% more than vehicle database model	3	1
28) Mich10a1, unknown to guidance, first flight aerodynamics mismodeling: aerodynamic lift coefficient 20% less and aerodynamic drag is 20% more than vehicle database model	3	1

[a]DOF: degrees of freedom.
[b]Mich10a1 and 10d1 are different X-33 missions (10d1 is a higher-energy flight). All environments are for the month of April unless noted.
[c]MCD: Monte Carlo dispersions.
[d]Different random seed indicates that a new random number was used to start the test case.
[e]PPO: power pack out (engine failure, time of failure indicated).
[f]Michael (nominal) and Ibex (low energy) are X-33 landing sites.
[g]ISS: International Space Station.
[h]LEO: low Earth orbit.

Table 2 Motivation for the tests

Tests	Motivation
1–4	Nominal X-33 missions with dispersions; test robustness to dispersions
5–9	Engine failures; test robustness to large off-energy cases and alternate landing sites
10–12	Large thrust dispersions; evaluate ability to maximize probability of successful landing
13–21	Entry from orbit; evaluate ability to adapt to different heating requirements and crossrange requirements with dispersions
22–25	Evaluate effects from failures causing a change in maneuverability; also shows robustness to changing vehicle models
26–28	Evaluate the effects of mis-modeling of aerodynamics on first flight; also shows robustness to changing vehicle models

Next, we describe the random dispersions of the Monte Carlo simulations. Aerodynamic-moment coefficients, hinge-moment coefficients, moments of inertia, RCS thrusters, main engine moments, slosh, and aerosurface actuators were dispersed for six-DOF runs only (tests 1–4). Ascent parameters are not dispersed for tests 13–21. Most parameters were randomly dispersed according to a normal distribution with variations set by the X-33 program. Some dispersions followed more complicated variations as needed for the X-33 high-fidelity models. Dispersed parameters are as follows:

1) Aerodynamic (function of Mach, angle of attack): lift, drag, pitch moment, body flap pitch moment, elevon pitch moment, pitch moment caused by pitch rate, side force caused by sideslip, roll moment caused by sideslip, yaw moment caused by sideslip, side force caused by body flap, roll moment caused by body flap, yaw moment caused by body flap, side force caused by elevon, roll moment caused by elevon, yaw moment caused by elevon, side force caused by rudder, roll moment caused by rudder, yaw moment caused by rudder, roll moment caused by roll rate, roll moment caused by yaw rate, yaw moment caused by roll rate, yaw moment caused by yaw rate.

2) Atmosphere: Global Reference Atmosphere Model (GRAM 99): random correlated densities and winds.

3) Hinge-moment coefficients (function of Mach, angle of attack): body flap, rudder, inboard elevon, outboard elevon.

4) RCS interference effects, each thruster (different depending on thruster location): normal force, side force, pitch moment, yaw moment, roll moment.

5) Mass properties: inert mass, center of gravity, moments of inertia, loaded liquid oxygen, loaded liquid hydrogen, propellant residuals, propellant utilization system liquid-oxygen measurement error, propellant utilization system liquid-hydrogen measurement error.

6) Navigation (function-of-flight phase): position bias, velocity bias, acceleration bias, angular rate bias, attitude error bias, heading error bias.

7) RCS thrusters, each thruster: thrust, mixture ratio, specific impulse, propellant load, thruster alignment.

8) Main engine: force from thrust in each direction (function of altitude), aerodynamic moment from thrust about each axis (function of altitude), fuel flow rate, oxidizer flow rate, mixture ratio, specific impulse (function of altitude), engine alignment.

9) Slosh: slosh mass, mass location, frequency, damping.

10) Aerosurface actuators, each surface, each sensor: position sensor gain and bias.

11) Thermal indicators (each body point): laminar vs turbulent flow.

12) Engine plume effects (function of Mach): lift, drag, pitch moment, roll moment, yaw moment, side force.

Automated Scoring

The phase 1 test evaluation involved a number of guidance and control experts reviewing the results (both graphical and numerical) and determining how well the method flew the vehicle. This approach worked, but had two drawbacks: 1) it requires a large amount of engineer time for evaluation of many parameters on many tests for multiple algorithms, and 2) the final evaluation has some subjectivity in it (and could potentially result in uneven evaluation). There was a benefit to this method, however. In evaluating the methods, it became clear to the evaluators what parameters were important to them and what values of these parameters were acceptable. The result was the ability to automate the scoring process for the phase 2 tests.

Tests are numerically scored, and then each test is weighted, with the scores added, so that the algorithms have a final numerical score. Normalization results in a perfect score being given a value of 1.0. For each parameter to be tested, there is a weight, and these multiply that parameter's score and add into the total. Single tests (not Monte Carlo dispersions) are scored as in this example:

Normal acceleration (the maximum normal acceleration value for the entire entry trajectory): 0–3.5g, 1.0–2.5g means the score is 1.0 for normal acceleration magnitudes below 2.5, 0.0 for values above 3.5, and linearly varying in between the two limit values. The parameter score is multiplied by the weight for that parameter (normal acceleration) and added into the total score for that test.

For Monte Carlo dispersion tests, the overall score is the average of the individual scores. A final criteria used for the tests concerns accuracy in reaching the TAEM targets. If the range, altitude, and heading angles are not sufficiently controlled in order to be able to land successfully, the test was considered a failure (score of 0) even if other criteria were met. Typical values used for the required accuracy at hitting the TAEM condition were $\pm$12.96 km (7 nm) for range, 2.1336 km (7000 ft) for altitude, and 10 deg for flight-path angle. If more than 10% of Monte Carlo cases fail to meet these TAEM conditions, then the entire Monte Carlo run is given a score of 0.0. Exceptions to this last criterion were tests 5 and 8. The 90% success criteria resulted in all algorithms failing these two tests. By removing the criteria, it became possible to see the relative scores of the various algorithms and thus to have a means for comparing them.

Table 3 lists the criteria compared for each of the various tests.

Results

Results of the tests are shown in the figures. These tests have been performed a number of times, with the algorithm designers given a chance to correct problems in their method's performance during the process. The algorithm developers spent substantial effort improving the algorithm performance in the testing. The baseline entry guidance is shown for comparison for tests where it is set up to fly the vehicle.

Figure 1 shows the performance for the entry guidance test cases. A score of 0.0 means that the algorithm failed the test. If more than one algorithm failed the test, a slightly negative score is used so that the reader is able to see the scores in the figure. The X-33 baseline guidance is used for tests 1–12 only. It is clear that it performs quite poorly as compared to the other algorithms. The reason for this is clearly visible in Fig. 2, which shows results from test case 1. The nominal TAEM interface altitude and range are 29.344 km (96,274 ft) and 55.56 km (30 nm), respectively. Although the baseline guidance has values generally clustered in this vicinity, the spread is significantly greater than the LQR TAEM spread, which is very tight around the nominal values. Four of the 100 cases for the baseline are off the graph, and others would not be land-able. The particular failed criterion in this case is that at least 90% of cases must be within 12.96 km (7 nm) of the desired TAEM range condition.

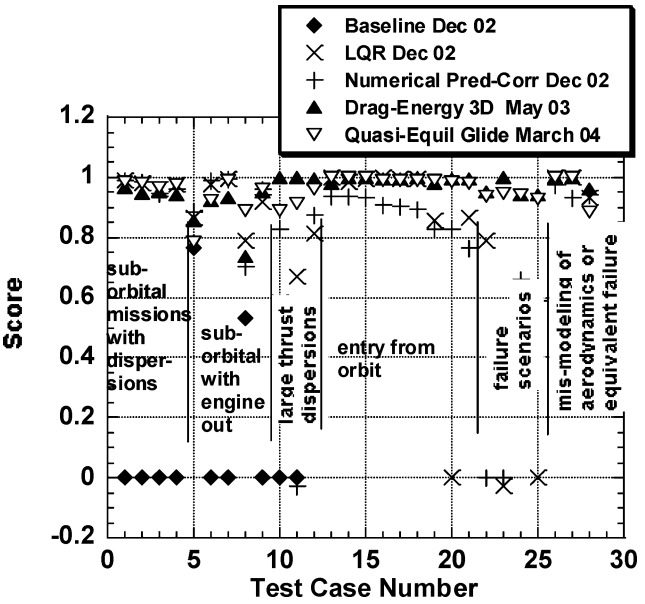

Fig. 1 Entry guidance test scores.

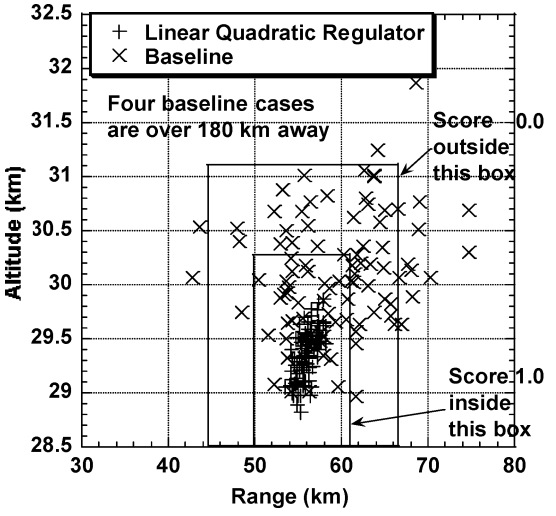

Fig. 2 Altitude vs range comparison for entry guidance (test case 1).

Although this baseline algorithm would be completely acceptable for flying a typical shuttle entry profile that has a long time available for removing dispersions as well as a benignly designed trajectory, the guidance for this X-33 suborbital case was required to remove ascent dispersions on a relatively sporty entry profile (an entry profile that includes a nonsmooth drag curve and requires significant maneuvering to follow) in a much shorter period of time. This might be necessary in some downrange abort scenarios for an orbital vehicle where using all of the fuel means that the energy will be quite off nominal for the entry phase of flight.

One reason the different performance in Fig. 2 makes sense is that the LQR alpha and bank gains/loops are designed together so that alpha "knows" what bank is doing and vice versa, causing them to work together more effectively. So we would expect better performance from the LQR method. Also, more tuning work with the baseline guidance might have produced somewhat better performance than what we actually obtained, but one of the advantages of LQR is that less tuning work is necessary.

The LQR algorithm scores fairly well across the board, although it fails some of the more difficult cases, probably because it does not have a trajectory profile tailored more to that case. Test case 20

Table 3 Test criteria[a]

Criteria number	Criteria description	Entry guidance test numbers[b]	Scoring weight	Scoring parameters[c]	Nominal values (for ± scoring parameters)
1	Deflection, body flap	$_{(1–4)}X^{(AvgTS)}$[d]	Tests 1–4: 0.04	Tests 1–4: 0-saturated >30 s, 1–0 s	——
2	Deflection, elevon	$_{(1–4)}X^{(AvgTS)}$	Tests 1–4: 0.04	Tests 1–4: 0-saturated >30 s, 1–0 s	——
3	Q-alpha, psf-deg	$X^{(Mx)}$[e]	Tests 1–21: 0.05 Tests 22–28: 0.03	Tests 1–2: 0–7500, 1–6500 Tests 3–4, 10, 13–28: 0–8000, 1–7000 Test 5: 0–8000, 1–7500 Test 6–9, 12: 0–7500, 1–6500 Test 11: 0–8200, 1–7500	——
4	Normal acceleration (maximum negative, *g*)	$X^{(Mn)}$[f]	Tests 1–4: 0.05 Tests 5–12, 16–21: 0.08 Tests 13–15: 0.1 Tests 22–28: 0.03	Tests 1–2, 6–9, 12: 0–3.5, 1–2.5 Tests 3–4: 0–4, 1–3.5 Test 5: 0–4.2, 1–3.6 Tests 10, 22–28: 0–4.0, 1–3.0 Test 11: 0–4.2, 1–3.7 Tests 13–21: 0–3.5, 1–3.0	——
5	Altitude, m (kft)	$X^{(TAEM)}$	Tests 1–4: 0.15 Tests 5–15: 0.16 Tests 16–21: 0.14 Tests 22–28: 0.21	Tests 1–4, 6–10, 13–21: 0–±1829 (6), 1–±915 (3) Tests 5, 11, 12, 22–28: 0–±2134 (7), 1–±1219 (4)	Tests 1–2, 5–8, 10–12, 22, 23, 26–28: 29345 (96.274) Tests 3–4, 9, 24, 25: 29438 (96.581) Tests 13–15: 30428 (99.827) Tests 16–21: 29432 (96.560)
6	Range to HAC, km (nm)[g]	$X^{(TAEM)}$[h]	Tests 1–4: 0.2 Tests 5–15: 0.23 Tests 16–21: 0.19 Tests 22–28: 0.28	Tests 1–4, 6–10, 13–21: 0–±11.112 (6), 1–± 5.556 (3) Tests 5, 11: 0–±14.816 (8), 1–±9.26 (5) Test 12: 0–±148.16 (80), 1–±111.12 (60) Tests 22–28: 0–±14.816 (8), 1–±7.408 (4)	Tests 1–11, 13–28: 55.56 (30) Test 12: 0 (0)
7	Flight-path angle, deg	$X^{(TAEM)}$	Tests 1–4: 0.05 Tests 5–12, 16–28: 0.06 Tests 13–15: 0.08	Tests 1–28: 0–±12, 1–±9	−13
8	PLAD pressure, N/m^2 (psi)[i]	$_{(1–4)}X^{(TAEM)}$	Tests 1–4: 0.04	Tests 1–4: 0–2.413e7 (3500), 1–2.758e7 (4000)	——
9	Bank angle (absolute value, deg)	$X^{(TAEM)}$	Tests 1–4: 0.04 Tests 5–28: 0.06	Tests 1–28: 0–60, 1–50	——
10	Heading error to HAC, deg	$X^{(TAEM)}$	Tests 1–4 : 0.1 Tests 5–15: 0.13 Tests 16–21: 0.11 Tests 22–28: 0.19	Tests 1–21: 0–±10, 1–±5 Tests 22–28: 0–±10, 1–±7	0 deg
11	RCS propellant used, kg (lbm)[j]	$_{(1–4)}X^{(TAEM)}$	Tests 1–4: 0.04	Tests 1–4: 0–226.8 (500), 1–181.4 (400)	——
12	Thermal-structural indicators, body points (1.0 is acceptable, uses thermal indicator model for X-33)	$_{(1–12;22–28)}X^{(AvgMxBp)}$[k]	Tests 1–4: 0.1 Tests 5–12: 0.13 Tests 22–28: 0.07	Tests 1–2, 6–10, 12, 22–28: 0–1.3, 1–1.0 Tests 3–5: 0–2.0, 1–1.2 Tests 11: 0–1.4, 1–1.0	——
13	Creep indicators, body points (1.0 is acceptable, uses thermal indicator model for X-33)	$_{(1–12;22–28)}X^{(AvgMxBp)}$	Tests 1–12: 0.1 Tests 22–28: 0.07	Tests 1–9, 12: 0–1.2, 1–0.8 Tests 10, 22–28: 0–1.3, 1–1.0 Test 11: 0–2.0, 1–1.2	——
14	Peak heat rate, W/m^2 (BTU/ft^2/s)	$_{(13–21)}X^{(Mx)}$	Tests 13–15: 0.19 Tests 16–21: 0.31	Tests 13–15: 0–9.08e5 (80), 1–8.51e5 (75) Tests 16–21: 0–7.38e5 (65), 1–6.81e5 (60)	——

[a]Criteria listed are for individual tests. The scoring was based on the desired values (listed in the scoring parameters column) for each variable. To obtain composite Monte Carlo tests, use the table and sum the individual scores according to the description given in the automated scoring section.

[b]Criteria listed are for all tests unless limited to tests indicated, that is,

1) X: The criterion is used in all tests.

2) $_{(1–4)}X$: The criterion is used only in tests 1–4.

3) $X^{(TAEM)}$: The criterion is scored based only on its value at the TAEM interface.

4) $_{(1–4)}X^{(TAEM)}$: The criterion is used only in tests 1–4 and will be scored based only on its value at TAEM.

[c]Score 1.0 for being equal to or better than the value listed as 1; score 0.0 for being equal to or worse than the value listed as 0; linear in between.

[d]$_{(AvgTS)}$-score represents the average of the scores assigned for the total saturation time for each surface.

[e]$_{(Mx)}$-score represents the score assigned for the maximum value.

[f]$_{(Mn)}$-score represents the score assigned for the minimum value.

[g]HAC: heading alignment cone (used to align with the runway).

[h]TAEM: terminal-area energy-management interface, an ending point at about 762 m/s (2500 fps) relative speed.

[i]PLAD: pneumatic load assist device (augments electromechanical actuators when needed).

[j]RCS: reaction control system.

[k]$_{(AvgMxBp)}$-score represents the average of the scores assigned for the maximum value of each body point.

is a high crossrange case that LQR fails because it does not have a trajectory profile tailored to high crossrange. LQR would be a good choice for a simple, robust guidance that does not involve onboard trajectory design.

The numerical predictor-corrector method performs well, although it has some isolated problems. Its capability to design smooth new profiles, combined with a robust guidance that includes the LQR after the high heating region is passed, leads to robust performance. It fails some of the toughest tests. Further improvements would possibly have removed the failures, but likely would not have led to better performance than the two highest-performing methods.

The quasi-equilibrium glide approach and the drag-energy three-dimensional algorithm both performed extremely well. Both approaches passed all of the tests and performed well on all tests. The total scores for the various algorithms, as of the most recent testing, are listed in Table 4.

Note that the drag-energy three-dimensional algorithm was submitted separately for the different X-33 missions (10a1 and 10d1), whereas the quasi-equilibrium glide testing is for a single algorithm. Ultimately a single algorithm is necessary that is flexible enough to fly the different missions without modification.

The criteria graph (Fig. 3) shows the performance on the various criteria for each algorithm. The criteria are listed in Table 3. The performance is shown only for those tests that did not fail (did not score a zero on the test cases graph). The number of successful tests for each algorithm can be determined from the test cases graph. Because the baseline passed only three tests, its criteria numbers are not meaningful and are left out of the figure. All of the new algorithms performed fairly well against the various criteria. It is apparent from the figure that there are differences between algorithm performance for some of the criteria.

Table 4 Final algorithm scores

Algorithm	Score
Baseline	8.4 (out of a possible 50 as a result of being tested against tests 1–12 only)
Linear quadratic regulator	83.5
Numerical predictor-corrector	82.3
Drag-energy three dimensions	95.9
Quasi-equilibrium glide	95.7

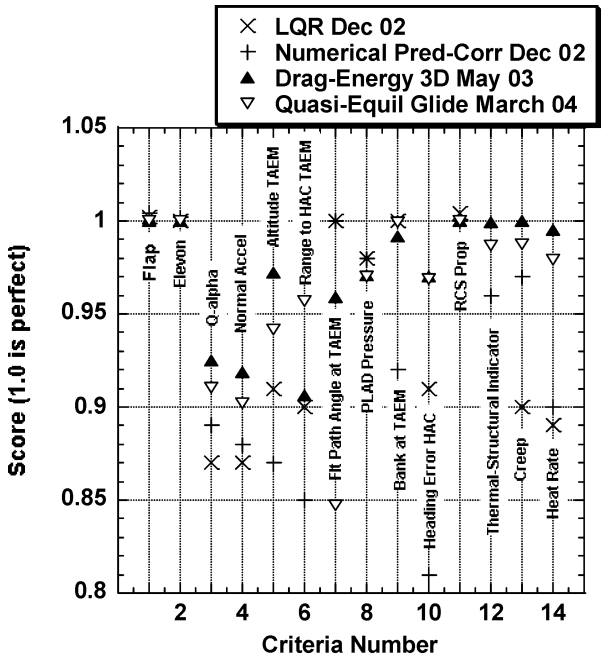

Fig. 3 Criteria scores.

Table 5 CPU time spent on first guidance call

Algorithm	CPU time, s
Baseline	0.000314
Linear quadratic regulator	$1.22E{-}05$
Numerical predictor-corrector	0.259041
Drag-energy three-dimensions	0.031893
Quasi-equilibrium glide	0.078994

Computational Intensity

The speed of computation of the various algorithms was measured in order to verify that they could be flown and used in real time. Table 5 shows the computer time spent on the first call to entry guidance for the Michael 10a1 trajectory:

The computer speed is 525×10^6 cycles per second. All subsequent calls to guidance used less CPU time than the first call. The numerical predictor-corrector, quasi-equilibrium glide, and drag-energy three-dimensional approaches used more time than the baseline and LQR methods because they calculated a new trajectory prior to flying it. In most cases, subsequent calls to guidance use far less CPU time than the first call. From the table, it is apparent that it should be possible to use any of these algorithms for real-time entry guidance. Trajectory generation takes more time, but should fit within computing capabilities of future onboard computers. The initial trajectory generation can be performed over a period of time if necessary, during the coast before entry guidance begins its closed-loop operation. The calls for guidance only and not trajectory generation should not tax the computer significantly. If trajectory generation is necessary after entry starts, it should be possible to accomplish it within the computing capabilities of the onboard computer, in a few guidance cycles if not in one (assuming a typical guidance cycle of one second). One issue is that the time taken to generate a trajectory, with iterations involved, can be variable. The preceding times are not necessarily the maximum that would ever be seen. This would need to be taken into account in developing the real-time system.

Conclusions

The primary contribution of this paper is to provide a quantitative comparison between the performance of five different entry guidance approaches. The methods were tested in high-fidelity simulation to determine their performance with respect to nominal missions, engine-out situations, dispersions, various failures, and vehicle mismodeling. All of the new approaches significantly outperformed the baseline entry guidance (current state-of-the-art) design. Improvement in safety results from the ability to adapt to unexpected significant off-nominal conditions and failure scenarios. This improvement is clearly shown by the test results. Improvement in cost results from the ability to use the methods for varying vehicle models and mission scenarios without significant effort expended. This improvement is also shown by the test results. The robustness with respect to different vehicle models was covered by significantly varying the maneuverability and aerodynamic parameters in the tests.

Expected flight processor capabilities should be able to handle the computational needs of the various algorithms tested. The quasi-equilibrium glide approach and the drag-energy three-dimensional method both performed extremely well. We believe they are now proven to the extent that they can be expected to work well on a future vehicle application. The linear quadratic regulator (LQR) approach, although having more difficulty with some of the tests as compared to the two top performers, is simpler computationally and would represent a good choice for a lower-risk approach in the sense that it involves less complicated software and mission success does not require an onboard converged trajectory design. The numerical predictor-corrector performed well and led to smooth flight profiles, but did not perform as well as the two with the highest scores. Further work might have enabled this approach to attain similar scores as the highest-scoring methods, but would have probably required increased parameter variations,

leading to increased computer run time, which was already the highest.

As of this writing, the drag-energy three-dimensional method is not a single algorithm, but has been delivered in three versions to cover the various test cases. It still needs to be modified so that it will be able to fly modified missions equally well without changing the algorithm.

There are a couple of issues that can be identified with the new entry guidance approaches. First, because the trajectory design process involves iteration it is likely to be a process that takes a variable length of time. This issue will have an impact on the real-time software design. Secondly, there is the issue of verifying that the new methods will never cause a vehicle to fail as a result of a failure to converge or some other reason with similar impact. Verification and reduction of risk could include showing that the new method flies all of the expected scenarios (different missions and dispersions) successfully, as well as expands the envelope to include successfully flying cases that would have previously failed. To further reduce risk, a nominal trajectory could be stored and used as long as conditions do not require a new trajectory. With that approach, the new method would only add to safety because it would only compute new trajectories in cases that would have failed (or would at least be near failure) previously. Software would need to be added to make the decision that a new trajectory is necessary.

Acknowledgments

The Advanced Guidance and Control Project was supported by the NASA X-33 Program Office. The Integration and Testing of Advanced Guidance and Control Technologies (ITAGCT) portion of the work was funded under the Space Launch Initiative and later by the Next Generation Launch Technologies Program.

References

[1]Hanson, J., "A Plan for Advanced Guidance and Control Technology for 2nd Generation Reusable Launch Vehicles," AIAA Paper 2002-4557, Aug. 2002.

[2]Hanson, J., "New Guidance for New Launchers," *Aerospace America*, Vol. 41, No. 3, 2003, pp. 36–41.

[3]da Costa, O., and Sachs, G., "Effects of Controls Degradation on Flight Mission of Reentry Vehicle," AIAA Paper 2002-4848, Aug. 2002.

[4]Hanson, J., "Advanced Guidance and Control Project for Reusable Launch Vehicles," AIAA Paper 2000-3957, Aug. 2000.

[5]Dukeman, G. A., "Profile-Following Entry Guidance Using Linear Quadratic Regulator Theory," AIAA Paper 2002-4457, Aug. 2002.

[6]Hanson, J., Jones, R., and Krupp, D., "Advanced Guidance and Control Methods for Reusable Launch Vehicles: Test Results," AIAA Paper 2002-4561, Aug. 2002.

[7]Hanson, J. M., Coughlin, D. J., Dukeman, G. A., Mulqueen, J. A., and McCarter, J. W., "Ascent, Transition, Entry, and Abort Guidance Algorithm Design for the X-33 Vehicle," AIAA Paper 98-4409, Aug. 1998.

[8]Zimmerman, C., Dukeman, G., and Hanson, J., "Automated Method to Compute Orbital Reentry Trajectories with Heating Constraints," *Journal of Guidance, Control, and Dynamics*, Vol. 26, No. 4, 2003, pp. 523–529.

[9]Chen, D. T., Saraf, A., Leavitt, J. A., and Mease, K. D., "Design and Evaluation of an Acceleration Guidance Algorithm for Entry," *Journal of Spacecraft and Rockets* (to be published).

[10]Shen, Z., and Lu, P., "On-Board Generation of Three-Dimensional Constrained Entry Trajectories," *Journal of Guidance, Control, and Dynamics*, Vol. 26, No. 1, 2003, pp. 111–121.

[11]Lu, P., "Regulation about Time-Varying Trajectories: Precision Entry Guidance Illustrated," *Journal of Guidance, Control, and Dynamics*, Vol. 22, No. 6, 1999, pp. 784–790.